Detection and imaging of the oxygen deficiency in single crystalline $YBa_2Cu_3O_{7-\delta}$ thin films using a scanning positron beam

M. Reiner,[1] T. Gigl,[1] R. Jany,[2] G. Hammerl,[2] and C. Hugenschmidt[1]
[1]*Lehrstuhl E21 at Physics Department and FRM II at Heinz Maier-Leibnitz Zentrum (MLZ), Technische Universität München, James-Franck Straße, 85748 Garching, Germany*
[2]*Experimental Physics VI, Center for Electronic Correlations and Magnetism, University of Augsburg, Universitätsstraße 1, 86135 Augsburg, Germany*

(Received 2 March 2015; accepted 11 March 2015; published online 20 March 2015)

Single crystalline $YBa_2Cu_3O_{7-\delta}$ (YBCO) thin films were grown by pulsed laser deposition in order to probe the oxygen deficiency δ using a mono-energetic positron beam. The sample set covered a large range of δ ($0.191 < \delta < 0.791$) yielding a variation of the critical temperature T_c between 25 and 90 K. We found a linear correlation between the Doppler broadening of the positron electron annihilation line and δ determined by X-ray diffraction. *Ab-initio* calculations have been performed in order to exclude the presence of Y vacancies and to ensure the negligible influence of potentially present Ba or Cu vacancies to the found correlation. Moreover, scanning with the positron beam allowed us to analyze the spatial variation of δ, which was found to fluctuate with a standard deviation of up to 0.079(5) within a single YBCO film. © *2015 AIP Publishing LLC*.
[http://dx.doi.org/10.1063/1.4916032]

High temperature superconductivity (HTS)[1] with a maximum transition temperature (T_c) of 92 K in $YBa_2Cu_3O_{7-\delta}$ (YBCO) (Refs. 2 and 3) is strongly influenced by the oxygen deficiency δ and the order of oxygen atoms (see, e.g., Refs. 4–6). Currently, for the development of new improved HTS materials based on cuprates ($T_c > 130$ K (Ref. 7)) and on iron-oxypnictides ($T_c = 55$ K for $SmO_{1-x}F_xFeAs$ (Refs. 8 and 9)), the amount of oxygen and hence the presence of oxygen vacancies is of outstanding importance.

Both the deeper understanding of the T_c (δ) dependence and the precise adjustment of T_c require information about the oxygen vacancies on a microscopic level. For this purpose, we studied YBCO thin film samples to gain fundamental insight into the elementary properties of the HTS. Thin films are extraordinarily suited since the application of pulsed laser deposition (PLD) using $SrTiO_3$ (STO) substrates enables epitaxial growth of YBCO in single crystalline quality with well defined stoichiometry. Beyond standard characterization techniques like electrical transport measurements, X-ray diffraction (XRD), or electron microscopy, positrons with their unique sensitivity to open-volume defects[10–12] reveal valuable additional information. So far, positron annihilation techniques have been applied in various studies to investigate YBCO bulk materials with positron lifetime spectroscopy,[13–16] measurement of the angular correlation,[17,18] and the Doppler broadening[19,20] of the annihilation radiation. In particular, positrons were found to be sensitive to the open volume formed by both metallic vacancies and oxygen deficiency in bulk samples of YBCO.[12,16]

In the present study, we applied depth dependent Doppler Broadening Spectroscopy (DBS) and Coincident DBS (CDBS) with a slow positron beam,[10,21] which allows us to probe films with a thickness of up to several hundreds of nanometers. DBS is particularly sensitive to the momentum of valence electrons, which has been reported to depend on the oxygen deficiency in YBCO.[17–20] For this reason, using a spatially resolving high-intensity positron beam enables both depth dependent measurements of δ and imaging of the lateral homogeneity in thin YBCO films. In addition, CDBS allows for elemental specific examination of atoms surrounding the open volume in YBCO. In order to emphasize the experimentally gained results, detailed calculations of CDB spectra taking into account metallic vacancies were performed.

YBCO thin films were grown at once by PLD on commercially available STO substrates ($10 \times 10\,mm^2$) using a KrF laser. The substrates were cut into four quadratic pieces, cleaned, heated up to 760 °C at a background oxygen pressure of 0.25 mbar for the thin film deposition and annealed at 400 mbar. Three samples (A2, A3, and A4) were individually heat treated at a constant temperature of 400 °C at different background pressures p_{temp} for varying times t_{temp} in order to adjust the oxygen deficiency (see Table I). One thin film sample was left as-grown (A1) as reference. The quality of the single crystalline YBCO films was routinely checked by XRD, and the c-axis parameter was evaluated by usual Θ-2Θ-scans for the determination of δ.[22] The spatial variation of δ designated by σ_δ was obtained from spatially resolved DBS (see below). Electrical transport measurements confirmed superconductive behavior for all samples (see T_c in Table I). The thickness of a YBCO film grown

TABLE I. Parameters of the $YBa_2Cu_3O_{7-\delta}$ thin films: The oxygen deficiency δ was determined by XRD; σ_δ describes the spatial variation of δ in the films obtained from spatially resolved DBS (Fig. 2); and T_c is the measured critical temperature.

Sample	δ	σ_δ	T_c (K)	t_{temp} (min)	p_{temp} (mbar)
A1	0.191	0.019(1)	90	n.a.	n.a.
A2	0.475	0.079(5)	60	30	$2\cdot10^{-2}$ (O_2)
A3	0.641	0.048(3)	60	30	10^{-7}
A4	0.791	0.031(2)	25	50	10^{-7}

under identical conditions was determined as 210 ± 10 nm by electron microscopy.

A mono-energetic beam enables depth dependent (C)DBS by implanting positrons with a kinetic energy E up to several keV into the specimen. The mean penetration depth $\bar{z}$ scales with E: $\bar{z} = \frac{A}{\rho} \cdot E^n$; A and n are material dependent parameters of the Makhovian implantation profile ($A = 3.76\ \mu g/(cm^2\ keV^n)$ and $n = 1.64$ for the examined system) and ρ is the mass density. After thermalisation within a few picoseconds, the positron diffuses through the sample before it annihilates with an electron after typically 100–200 ps. During diffusion, the positron can get trapped in attractive potential wells formed by open volume defects where the annihilation probability with core electrons is lower. Thus, the lower mean momentum of the annihilating electrons with the longitudinal component p_L^- leads to a smaller Doppler shift $\Delta E = \frac{1}{2} c\, p_L^-$ of the annihilation γ-quanta (c is the velocity of light). In DBS, ΔE is measured with high purity Ge detectors (energy resolution 1.4 keV at 511 keV). The Doppler broadening of the annihilation line is commonly evaluated by the lineshape parameter S, which is defined by the number of counts in the central region of the 511 keV photopeak (here $\Delta E < 0.84$ keV) divided by the total number of counts. The depth profiles $S(E)$ allow for the extraction of the positron diffusion length L_+, which is significantly reduced when positrons are trapped in open volume defects.

In CDBS, a strongly enhanced peak-to-background ratio is achieved by detecting both annihilation γ-quanta in coincidence.[23,24] Therefore, high Doppler shifts caused by the annihilation of core electrons can be measured and hence element-specific information of the atoms surrounding the annihilation site can be extracted. Usually, so-called ratio curves are analyzed which are obtained (after normalization) by dividing the measured CDB spectra with a reference spectrum (see, e.g., Ref. 25). The present measurements were performed with the CDB spectrometer[26] at the high-intensity positron beam at NEPOMUC.[27,28] The positron implantation energy ranges from 0.5 to 30 keV and spatially resolved measurements can be conducted by scanning the beam across the sample surfaces with a high spatial resolution of 0.3 mm for $E > 10$ keV.

For all specimens, the $S(E)$ depth profiles were measured (Fig. 1) in order to determine the fraction of positrons annihilating in the YBCO film with the aid of the VEPFIT program.[29] For the least square fits of all $S(E)$ curves, the two-layer YBCO/STO system including the surface was modeled and the respective S-parameters and positron diffusion lengths were fitted. Exemplary, the fit result for $S(E)$ of sample A3, which yielded the fraction of positrons annihilating in the YBCO film displayed in the color map of Fig. 1, is plotted as solid line. The steep increase of $S(E)$ towards the surface ($E < 1.7$ keV) is explained by the annihilation of positrons after back diffusion to the surface. The positron diffusion length L_+ was always found to be smaller than 5 nm, which is extremely short compared to typically 100 nm for defect-free metallic single crystals (see below). For high beam energies ($E > 7$ keV) an increasing fraction of positrons annihilates in the STO substrate and leads to the decrease of $S(E)$. The plateau in the range of $1.7 < E < 7$ keV is caused by the positron annihilation predominantly in the

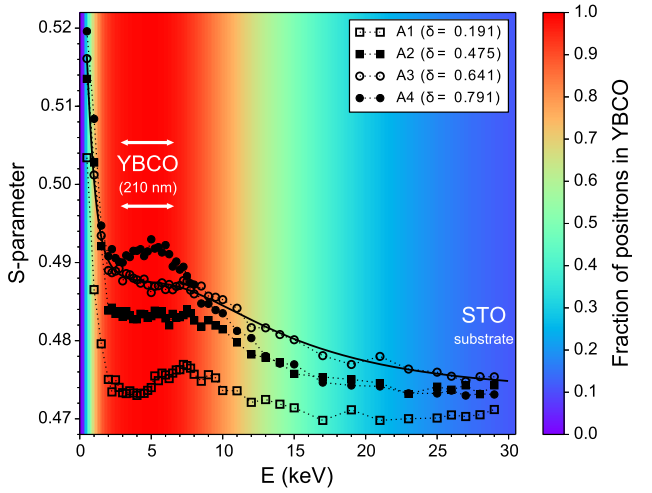

FIG. 1. $S(E)$ of the $YBa_2Cu_3O_{7-\delta}$ thin film samples: The fraction of positrons annihilating in the $YBa_2Cu_3O_{7-\delta}$ films as function of E is displayed by the color code, which was obtained by the fit shown for sample A3 (solid line).

YBCO film. Therefore, the S-parameter characteristic for each YBCO layer S_{YBCO} was determined by averaging the S values in the range of $3.25 \le E \le 6.25$ keV, where more than 98% of the positrons annihilate within the film. The very flat $S(E)$ dependence between 2 and 8 keV of specimen A2 is explained by a high homogeneity in depth of the YBCO film. In case of sample A1, where the difference between S_{YBCO} and the substrate S-parameter nearly vanishes, the slight increase for $4.5 < E < 7.5$ keV probably arises from the lattice mismatch (<2%) between YBCO and STO leading to a higher defect concentration at the interface. A similar but less distinct behavior is also observed in sample A4 between 3 and 6 keV.

In order to probe the structural homogeneity within the plane, spatially resolved DBS was performed by scanning the positron beam over the samples mounted on an Al sample holder (see S(x,y)-map in Fig. 2). The spatial resolution was 1 mm at the chosen implantation energy of 4 keV, where surface and interface effects can be neglected. For each specimen, a characteristic S-parameter S_{map} was determined by averaging the S values over the according area in the 2D map. Only a small difference between S_{map} and the depth averaged S-parameter S_{YBCO} was found that is explained by the differently probed depth. The dependencies of both S_{YBCO} and S_{map} on δ are astonishingly well described by a linear correlation (right plot in Fig. 2). A similar finding was reported for sintered YBCO bulk samples up to $\delta = 0.6$.[19]

The found correlation S_{map} (δ) is used to evaluate the spatial variation σ_δ of δ within the YBCO films. For this purpose, the spatial scattering of the S-parameter was statistically analyzed for each specimen. The standard deviation σ_{map} of the mean value S_{map} is assumed to comprise both the *true* spatial variation of the S-parameter σ_{sp} and the statistical error $\sigma_{st} = 1.16 \times 10^{-3}$ of the measured S values. Consequently, σ_{sp}, which is given by $\sigma_{sp} = \sqrt{\sigma_{map}^2 - \sigma_{st}^2}$, can be applied to estimate the spatial variation σ_δ of δ with $\sigma_\delta = 1/0.029(2)\sigma_{sp}$ using the fit equation shown in Fig. 2. It is noteworthy that tempering the YBCO films generally led to a significant increase of the spatial inhomogeneity of δ

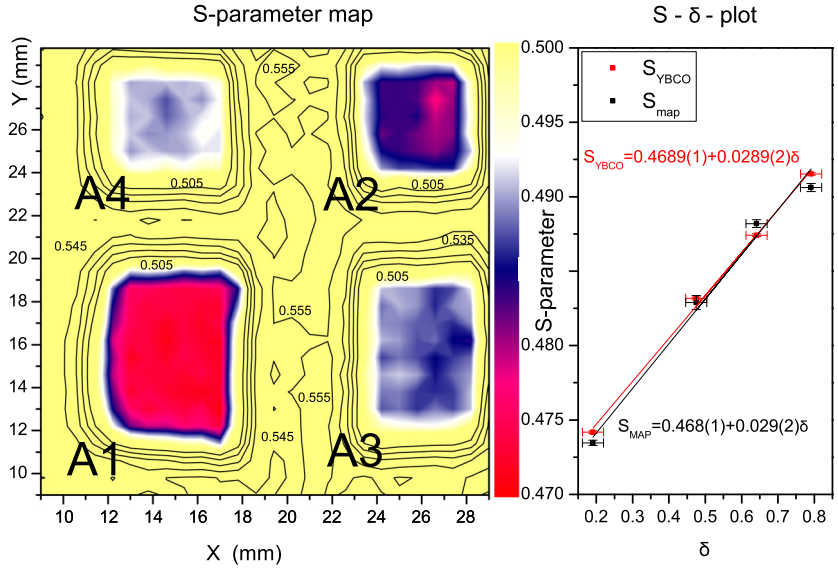

FIG. 2. 2D S-parameter map of the four YBCO samples obtained by spatially resolved DBS at $E = 4$ keV (left). Correlation between S-parameter and δ determined from XRD (right). The solutions of the linear fits are depicted as solid lines.

(see σ_δ values given in Table I). The fluctuation of $\sigma_\delta = 0.079(5)$ observed in sample A2 is a factor of four higher than in the non-tempered film A1. A closer look to the according S(x, y) distribution reveals a region of a lower oxygen deficiency on one side. Since sample A2 was the only one tempered in an oxygen atmosphere, the larger inhomogeneity could be attributed to a more complicated process of oxygen out diffusion.[30]

In order to analyze the correlation between the DBS results and δ in more detail, CDB spectra were recorded with an implantation energy of $E = 4$ keV. As shown in Fig. 3, the measured ratio curves with respect to the sample A4 show systematic changes with decreasing oxygen deficiency: (i) weakening for small electron momenta $p_L^- < 4 \cdot 10^{-3}\, m_0 c$, (ii) enhancement for $4 \cdot 10^{-3}\, m_0 c < p_L^- < 19 \cdot 10^{-3}\, m_0 c$, and hence higher core annihilation probability, and (iii) only tiny enhancement of the element-specific signature in the high momentum region $p_L^- > 19 \cdot 10^{-3} m_0 c$. All spectra $I_\alpha(p_L^-)(\alpha = A1, \ldots, A4)$ were fitted using a linear superposition with the weighting factor x_{CDB},

$$I_\alpha(p_L^-) = (1 - x_{CDB}) \cdot I_{A1}(p_L^-) + x_{CDB} \cdot I_{A4}(p_L^-). \quad (1)$$

The fit results (solid lines in Fig. 3) well describe the spectra, which essentially show the same signature with different amplitude. This observation is explained by a transition between two different positron states indicating that tempering of the films leads to a continuous transition from $YBa_2Cu_3O_{7.00}$ to $YBa_2Cu_3O_{6.00}$. In addition, there is no evidence for a drastic δ-dependent change in the structural ordering of oxygen atoms or of the chemical surrounding of the positron annihilation site. The comparison of the weighting factor x_{CDB} with both S_{YBCO} and δ reveals a strong linear dependence (see Fig. 3, left). Thus, it can be concluded that DBS and CDBS are clearly sensitive to the varying oxygen deficiency δ, and other effects such as trapping in metallic vacancies, if present, play only a minor role. For deeper understanding of this behavior, the measured CDB spectra are compared to calculated ones.

The CDB spectra were calculated by use of the MIKA Doppler program,[31] which describes the positron electron

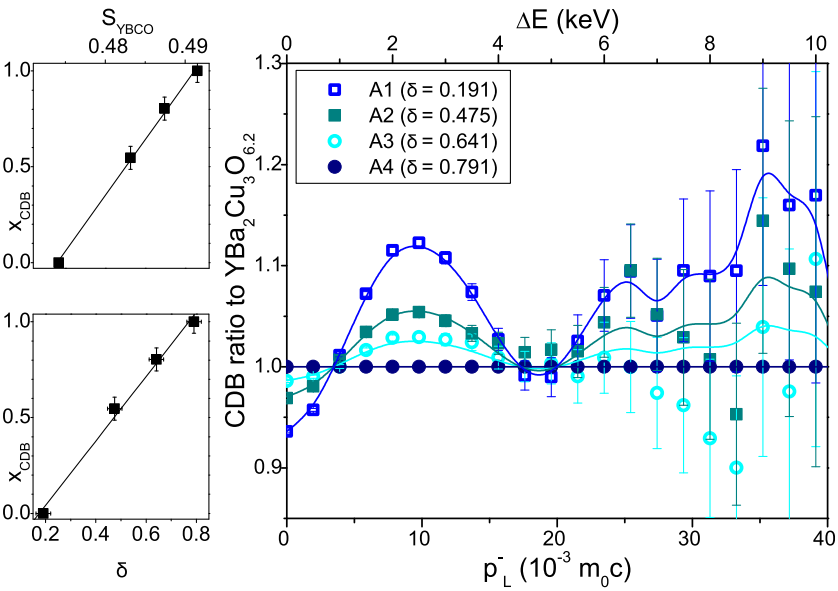

FIG. 3. Measured CDBS ratio curves of the YBCO thin film samples (right): The solid lines were obtained by a linear superposition of the spectra A1 and A4 with the fitted weighting factor x_{CDB}. The plots on the left show the linear correlation of x_{CDB} with S_{YBCO} and δ, respectively.

annihilation in a two-component density functional theory (DFT) frame in the limit of a vanishing positron density,[12] and is based on an atomic superposition method for electron wavefunctions.[32] The enhancement of the electron positron correlation is described by a generalized gradient approximation (as proposed by Barbiellini *et al.*[33]) with a parametrization based on data by Arponen and Pajanne.[34] All calculated spectra were convolved with a Gaussian in order to mimic the experimental energy resolution as described in Ref. 35.

The calculated ratio curve for defect free $YBa_2Cu_3O_{7.00}$ to $YBa_2Cu_3O_{6.00}$ (Fig. 4(b)) exhibits the same features as the measured ones in oxygen rich YBCO thin films. The corresponding 3D positron probability densities $|\Psi_+(\mathbf{r})|^2$ are plotted as isosurfaces in Fig. 4(a). The calculated 2D delocalized positron state in defect free YBCO is in agreement with the previous calculations[12,16,17,36–39] for both $\delta = 0$ and $\delta = 1$. Within the present calculations, the oxygen deficiency δ was varied between 0 and 1 under approximation of a tetragonal structure and accounting for the changing lattice constants. We confirmed that the positron probes the same region in YBCO, i.e., the plane of Cu atoms with more or less oxygen atoms in the Cu-O chains. This 2D delocalization of the positron causes a low mobility along the c-axis even in defect free YBCO and hence, could well explain the extremely low positron diffusions length of $L_+ < 5$ nm observed in the $S(E)$ depth profiles.

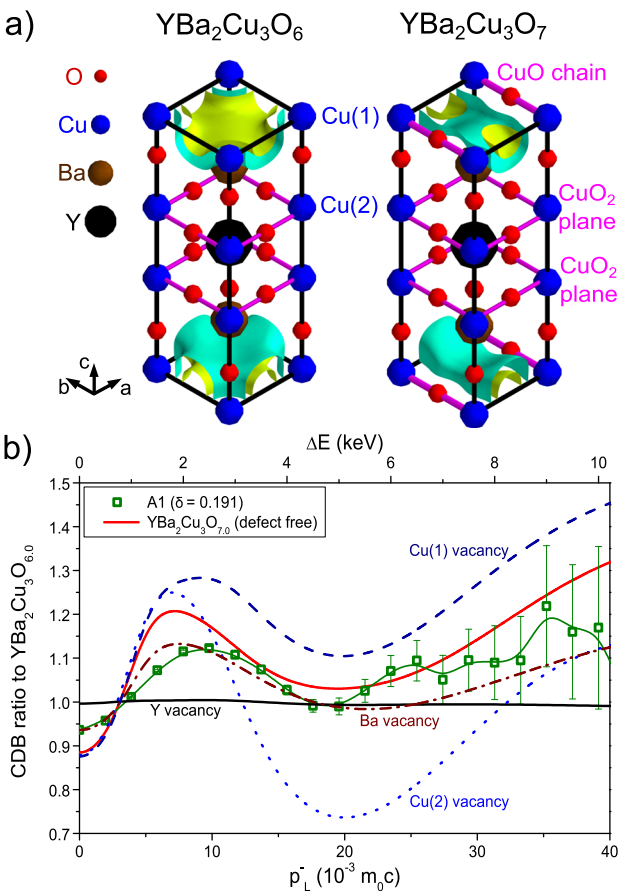

FIG. 4. (a) Calculated 3D isosurfaces of the positron probability density in YBCO (linear scale of the contours). (b) Calculated CDBS ratio curves for defect free YBCO and with different types of metallic vacancies (bold lines). The measured ratio curve of A1/A4 is shown for comparison.

Since metallic vacancies can also act as positron trapping sites,[16] their influence on the δ dependence of the CDB spectra was examined. For this purpose, the CDB ratio curve of $YBa_2Cu_3O_{7.00}$ to $YBa_2Cu_3O_{6.00}$ was calculated including the presence of various vacancy types (Fig. 4(b)). When the positron is trapped in a Y vacancy V_Y, the CDB spectra for $\delta = 0$ and 1 hardly differ and hence lead to a ratio curve equal to unity. Evidently, this behavior is in contrast to positron trapping in Ba vacancies V_{Ba} or in vacancies at the different Cu sites $V_{Cu(1)}$ and $V_{Cu(2)}$. The ratio curves for positron annihilation in V_{Ba} or in $V_{Cu(1)}$ exhibit similar features as that for defect-free YBCO. Despite being trapped in V_{Ba}, the positrons remain sensitive to the changing oxygen content in YBCO, and a positron attracted by a Cu(1) vacancy yields a more enhanced ratio curve above 7×10^{-3} m_0c. A more complex behavior was found for $V_{Cu(2)}$. In case of $YBa_2Cu_3O_{7.00}$, defect trapping clearly leads to the localization of the positron wave function in $V_{Cu(2)}$, whereas $V_{Cu(2)}$ in $YBa_2Cu_3O_{6.00}$ only leads to a tiny deformation of $|\Psi_+(\mathbf{r})|^2$, i.e., the positron still occupies the CuO plane in a 2D delocalized state. This effect drastically influences the shape of the obtained ratio curve which exhibits a deep minimum at 20×10^{-3} m_0c.

The measured δ-dependent ratio curves can be completely explained by annihilation in defect free YBCO. As revealed by the calculations, the amount of Y vacancies in the YBCO films (if at all) is negligible since positron annihilation in V_Y would be independent from δ and hence would not lead to the strong δ-dependence of the experimental results. On the contrary, the presence of Ba and Cu vacancies cannot be excluded due to the similarity of the according calculated ratio curves. However, it has to be emphasized that even in the case of positron trapping in these types of vacancies positrons still sensitively probe the oxygen deficiency in YBCO.

In this letter, we demonstrated that (C)DBS using a slow positron beam is a powerful tool for probing the oxygen deficiency in thin film oxides. The experimental results obtained for YBCO thin films reveal a strong correlation of the Doppler broadening of the positron annihilation line to the oxygen deficiency δ determined by XRD. Backed by calculated CDB spectra, the found linear dependence can be well explained by the positron affinity to the oxygen deficient plane in the defect free YBCO crystal structure. According to the calculations, surprisingly, a similar dependence can be expected when the positron is trapped in a Ba or Cu vacancy. The presence of Y vacancies was found to be unlikely since trapping in this type of vacancy would suppress the positron sensitivity to δ. Finally, we succeeded to image and to analyse the spatial distribution of the oxygen deficiency quantitatively using the scanning positron beam: A minimum spatial variation of δ with $\sigma_\delta = 0.019(1)$ was found in the as-deposited film, whereas the δ fluctuation in tempered films was found to be up to four times larger.

Financial support was gratefully acknowledged within the Project Nos. BMBF 05K13WO1 and DFG TRR 80.

[1]J. Bednorz and K. Müller, Z. Phys. B: Condens. Mater. **64**, 189 (1986).
[2]M. K. Wu, J. R. Ashburn, C. J. Torng, P. H. Hor, R. L. Meng, L. Gao, Z. J. Huang, Y. Q. Wang, and C. W. Chu, Phys. Rev. Lett. **58**, 908 (1987).

[3]S. Hikami, T. Hirai, and S. Kagoshima, Jpn. J. Appl. Phys., Part 2 **26**, L314 (1987).
[4]R. Liang, D. A. Bonn, and W. N. Hardy, Phys. Rev. B **73**, 180505 (2006).
[5]T. A. Zaleski and T. K. Kopeć, Phys. Rev. B **74**, 014504 (2006).
[6]V. Matic, N. Lazarov, and M. Milic, J. Alloys Compd. **551**, 189 (2013).
[7]J. D. G. A. Schilling, M. Cantoni, and H. R. Ott, Nature **363**, 56 (1993).
[8]R. Zhi-An, L. Wei, Y. Jie, Y. Wei, S. Xiao-Li, L. Zheng-Cai, C. Guang-Can, D. Xiao-Li, S. Li-Ling, Z. Fang, and Z. Zhong-Xian, Chin. Phys. Lett. **25**, 2215 (2008).
[9]R. Zhi-An, L. Wei, Y. Jie, Y. Wei, S. Xiao-Li, L. Zheng-Cai, C. Guang-Can, D. Xiao-Li, S. Li-Ling, Z. Fang, and Z. Zhong-Xian, EPL **83**, 17002 (2008).
[10]P. J. Schultz and K. G. Lynn, Rev. Mod. Phys. **60**, 701 (1988).
[11]R. N. West, Adv. Phys. **22**, 263 (1973).
[12]M. J. Puska and R. M. Nieminen, Rev. Mod. Phys. **66**, 841 (1994).
[13]C. Q. Tang, B. R. Li, and A. Chen, Phys. Rev. B **42**, 8078 (1990).
[14]H. Hermes, M. Forster, and H.-E. Schaefer, Phys. Rev. B **43**, 10399 (1991).
[15]K. O. Jenson, R. M. Nieminen, and M. J. Puska, J. Phys.-Condens. Mater. **1**, 3727 (1989).
[16]R. M. Nieminen, J. Phys. Chem. Solids **52**, 1577 (1991).
[17]E. C. von Stetten, S. Berko, X. S. Li, R. R. Lee, J. Brynestad, D. Singh, H. Krakauer, W. E. Pickett, and R. E. Cohen, Phys. Rev. Lett. **60**, 2198 (1988).
[18]M. Peter and A. A. Manuel, Phys. Scr. **1989**, 106.
[19]L. Smedskjaer, B. Veal, D. Legnini, A. Paulikas, and L. Nowicki, Physica B+C **150**, 56 (1988).
[20]S. G. Usmar, P. Sferlazzo, K. G. Lynn, and A. R. Moodenbaugh, Phys. Rev. B **36**, 8854 (1987).
[21]P. Coleman, *Positron Beams and Their Applications* (World Scientific, 2000).
[22]P. Benzi, E. Bottizzo, and N. Rizzi, J. Cryst. Growth. **269**, 625 (2004).
[23]P. Asoka-Kumar, M. Alatalo, V. J. Ghosh, A. C. Kruseman, B. Nielsen, and K. G. Lynn, Phys. Rev. Lett. **77**, 2097 (1996).
[24]P. E. Mijnarends, A. C. Kruseman, A. van Veen, H. Schut, and A. Bansil, J. Phys. Condens. Mater. **10**, 10383 (1998).
[25]P. Pikart and C. Hugenschmidt, Nucl. Instrum. Methods Phys. Res., Sect. A **750**, 61 (2014).
[26]M. Reiner, P. Pikart, and C. Hugenschmidt, J. Phys. Conf. Ser. **443**, 012071 (2013).
[27]C. Hugenschmidt, B. Loewe, J. Mayer, C. Piochacz, P. Pikart, R. Repper, M. Stadlbauer, and K. Schreckenbach, Nucl. Instrum. Methods Phys. Res., Sect. A **593**, 616 (2008).
[28]C. Hugenschmidt, C. Piochacz, M. Reiner, and K. Schreckenbach, New J. Phys. **14**, 055027 (2012).
[29]A. van Veen, H. Schut, M. Clement, J. M. M. de Nijs, A. Kruseman, and M. R. IJpma, Appl. Surf. Sci. **85**, 216 (1995).
[30]J. R. LaGraff and D. A. Payne, Phys. Rev. B **47**, 3380 (1993).
[31]T. Torsti, T. Eirola, J. Enkovaara, T. Hakala, P. Havu, V. Havu, T. Höynälänmaa, J. Ignatius, M. Lyly, I. Makkonen, T. T. Rantala, J. Ruokolainen, K. Ruotsalainen, E. Räsänen, H. Saarikoski, and M. J. Puska, Phys. Status Solidi B **243**, 1016 (2006).
[32]M. J. Puska and R. M. Nieminen, J. Phys. F: Met. Phys. **13**, 333 (1983).
[33]B. Barbiellini, M. J. Puska, T. Torsti, and R. M. Nieminen, Phys. Rev. B **51**, 7341 (1995).
[34]J. Arponen and E. Pajanne, Ann. Phys. **121**, 343 (1979).
[35]M. Reiner, T. Gigl, and C. Hugenschmidt, J. Phys. Conf. Ser. **505**, 012025 (2014).
[36]D. Singh, W. E. Pickett, R. E. Cohen, H. Krakauer, and S. Berko, Phys. Rev. B **39**, 9667 (1989).
[37]P. E. A. Turchi, A. L. Wachs, K. H. Wetzler, J. H. Kaiser, R. N. West, Y. C. Jean, R. H. Howell, and M. J. Fluss, J. Phys. Condens. Mater. **2**, 1635 (1990).
[38]T. McMullen, P. Jena, S. N. Khanna, Y. Li, and K. O. Jensen, Phys. Rev. B **43**, 10422 (1991).
[39]P. E. Mijnarends and A. Bansil, "Theory of electron and positron momentum distributions in solids," in *Positron Spectroscopy of Solids: Proceedings of the International School of Physics* "*Enrico Fermi*" (1993), Vol. 125.